# High resolution time-of-flight positron emission tomograph.



doi: 10.1063/1.1141549

# High resolution time-of-flight positron emission tomograph

Keizo Ishii and Hikonojo Orihara
*Cyclotron and Radioisotope Center, Tohoku University, Aramaki-Aoba, Aoba-ku, Sendai 980, Japan*

Taiju Matsuzawa
*Research Institute for Tuberculosis and Cancer, Tohoku University, Seiryocho, Aoba-ku, Sendai 980, Japan*

David M. Binkley and Ronald Nutt
*CTI PET Systems, Inc., 810 Innovation Drive, Knoxville, Tennessee 37932*

(Received 2 May 1990; accepted for publication 18 July 1990)

A time-of-flight positron emission tomograph (TOF-PET) was recently developed for the purpose of clinical medical study and brain research. It provides high-quality positron images with a spatial resolution of 8 mm full width at half-maximum (FWHM) which is obtained by the use of time-of-flight (TOF) location techniques and small $10\times18$-mm $BaF_2$ detectors to detect the positron-electron annihilation $\gamma$-rays. The time-of-flight resolving time was 623 ps (FWHM) in the system, which has improved the S/N ratio for positron images. This new TOF-PET has been designed to digitally record the arriving time of $\gamma$-rays at the detectors using the system clock. With this method, the architecture of hard and software for taking TOF sinograms and reconstructing TOF images is simplified compared to that of other TOF-PET systems. The details of this system are described here.

## I. INTRODUCTION

Positron-computed tomography or positron emission tomography (PET)[1-3] provides images of an organ's function, in contrast to x-ray computed tomography (CT) and magnetic resonance imaging (MRI) which image an organ's physical characteristics. By using a cyclotron, short-lived, positron-emitting radioisotopes of $^{11}C$, $^{13}N$, $^{15}O$ or $^{18}F$ for labeling glucose, galactose or other chemical compounds can be produced for injection into the human body. The quantity of positron-emitting radioisotopes accumulated in an organ through metabolism can be estimated by coincidence events of a pair of $\gamma$-rays produced from their positron annihilations. This enables a quantitative examination of the functions of the brain, heart and other organs for the diagnosis of dementia, Alzheimer disease, brain infarction, cardiac disease and cancer.[4]

Positrons emitted from the radioisotopes in a body travel a short range (i.e., 3 mm for $^{18}F$) and by their annihilation with electrons produce a pair of $\gamma$-rays with equal energy of 511 keV which are emitted in an opposite direction from each other. The images of spatial distribution of positron emitting nuclides can be obtained from the coincidence lines formed by the pair of $\gamma$-rays by means of an image-reconstruction method similar to that of x-ray CT and MRI. In the case of a low activity region close to a high activity region, the images are reconstructed including the noise induced by the statistical errors of positron events in the high activity region. This difficulty may be reduced however by using the time-of-flight location on coincidence lines in the image reconstruction. In principle, the position of annihilation can be determined from the difference between the time of flights of the $\gamma$-rays

$$x=\frac{1}{2}(t_2-t_1)\times C, \tag{1}$$

where $x$ is the distance from the middle point between detectors 1 and 2 which face each other, $t_{1(2)}$ is the time of flight of $\gamma$-ray from the position of annihilation to the detector 1(2) and $C$ the light velocity. The use of a fast decay component of light from a $BaF_2$ or CsF scintillator enables such a coincident measurement, while it is impossible for $Bi_4Ge_3O_{12}$ (BGO) and NaI scintillators which are used in a conventional PET. The positron emission tomograph based on this idea is called a time-of-flight (TOF)PET which provides high quality images with a good S/N ratio.[5,6] The reduced TOF-PET will permit us to find delicate or fine changes in metabolism in the presence of a strong background. For this reason, The TOF-PET was constructed.

The development of TOF-PET was initiated by the groups of Washington University[7,8] and Laboratoire d'Electronique et de Technologie de l'Informatique (LETI).[9,10] In the early development of TOF-PET, they have used a scintillator of CsF which is a deliquescant crystal with a decay time constant of 2.5 ns. Laval and his coworkers discovered a $BaF_2$ scintillator which can improve the time resolution of TOF-PET over the CsF scintillator.[11] The $BaF_2$ scintillator is not deliquescent and emits the photons with a decay time constant of 650 ps of which the wavelength is 220 nm. Photons of short wavelength are heavily absorbed with a glass window but they can pass through a quartz window. For this reason, the $BaF_2$ scintillator should be coupled to the photomultiplier with a quartz window. In the first of TOF-PETs, Super Positron emission transaxial tomograph (PETT)[8] of Washington University and TTV01[10] of LETI, photomultipliers with a large diameter of one inch and correspondingly large detector crystals as used which resulted in a poor spatial resolution of 11 mm FWHM. The method of coupling 8 small $BaF_2$ scintillators to 5 photomultipliers was devised in order to obtain a high spatial resolution.[12,13] On the other hand, photomultipliers with a small diameter of 10 mm (Hamamatsu R2496) were recently obtainable on the market and by using them the spatial resolution of TOF-PET can be improved.[14]

 0034-6748/90/123755-08$02.00  

For the purpose of constructing the TOF-PET, new techniques were developed for coincident measurements[15] of positron $\gamma$-rays with the $BaF_2$ scintillators and for image reconstruction[16] of three dimensional sinograms. In order to obtain accurate measurement of time-of-flight, electronic circuits consisting of constant fraction discriminators (CFD) and time digitizers with time channels 62.5 ps were designed.[17] By modifying the coincidence processor[18] and real time sorter[19] of a conventional PET PT931[20] to define TOF sinograms, its data taking system was used for the TOF-PET. Additionally, new computer programs for data taking, image reconstruction, system operation and other functions of the TOF-PET were developed. The system details and measured performance of this newly developed TOF-PET are presented here.

## II. SYSTEM DESCRIPTION

The TOF-PET consists of a gantry, data-acquisition system and data processing system which are shown in Fig. 1.

### A. Gantry

The gantry currently consists of one detector ring with 16 detector buckets each having 16 $BaF_2$ scintillation detectors. It is possible to upgrade the present gantry from one ring to multiple rings. The multiple ring TOF-PET will provide high quality three dimensional images reconstructed with the additional coincidence lines with respect to the axial direction. Observation of various views in three dimensional images will be useful for studies on organic function and metabolism. The total number of detectors is 256 per ring and the diameter of detector ring, that is, the distance from a surface of detector to that of an opposite side is 102 cm. Lead plates between detectors are used to define a detector width and also shield them from scattered $\gamma$-rays. The $BaF_2$ crystal has a polyhedron shape shown in Fig. 2 and is covered with a Teflon tape and $TiO_2$ powder which reflects the photons of the fast decay component well. The photomultipliers, with a quartz window of 10 mm in diameter (Hamamatsu R2496),

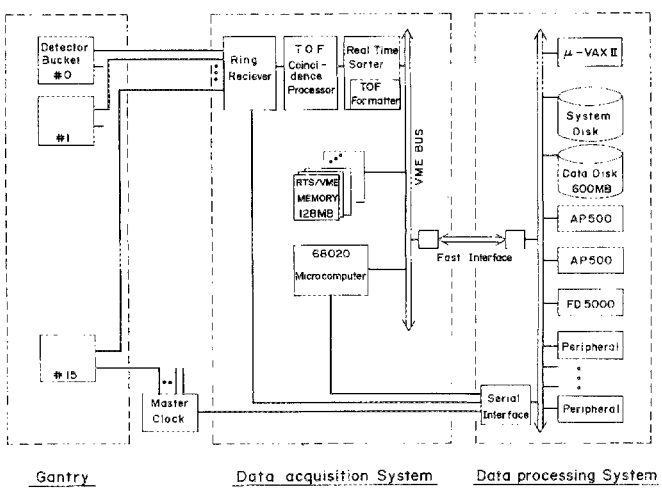


FIG. 1. Block diagram of the TOF-PET.

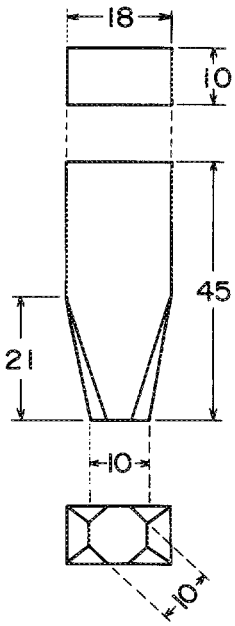


FIG. 2. Design of $BaF_2$ crystal. The crystal is a dodecahedron of which surfaces are well polished.

are coupled to $BaF_2$ crystals with a transparent liquid silicone rubber compound (RTV). The coupling between photomultiplier and $BaF_2$ crystal is quite stable, and during this one year, there were only two detector problems, these being failures of photomultiplier tubes.

Anode signals of the photomultipliers are fed to a newly designed CFD which produces fast timing signals. Detector signal discrimination in the CFD is used to suppress low energy $\gamma$-rays. In the case of a $BaF_2$ scintillator, the percentage of photopeak to total yields is 20% for the $\gamma$-rays of 511 keV, while it is 42% for BGO. Accumulating only the photopeak is desired for reduction of background induced by scattered $\gamma$-rays, however, a threshold level of 250 keV was adopted to improve detector efficiency. The time when a $\gamma$-ray arrives at a photomultiplier is recorded by a time digital converter (TDC) using system clock pulses of 16 ns and 256 ns in periods. Arriving time and detector numbers are transferred from detector buckets to a ring receiver in the data-acquisition system. Figure 3 represents a block diagram of detector bucket. The fast detector timing pulses are processed at each detector bucket, as mentioned later, all detector time axes can be adjusted so as to coincide with that of a reference detector. In the case of other TOF-PET systems,[8,10,12,14,21] fast detector timing pulses are processed by time-to-analog converters (TAC) outside of the gantry.

A large patient opening (90 cm) is used to measure simultaneous patient emission and transmission source using the TOF technique. The TOF technique permits a separation between emission and transmission events. The gantry can be wobbled with an orbit of 12.4 mm in diameter for high resolution studies. It is also possible to tilt ($\pm$ 30°) and rotate the gantry.

### B. Data-acquisition system

The ring receiver, coincidence processor and real-time sorter (RTS) of the PT931 conventional PET are used in the data-acquisition system of the present TOF-PET. The coincidence processor, however, is modified to record TOF in-

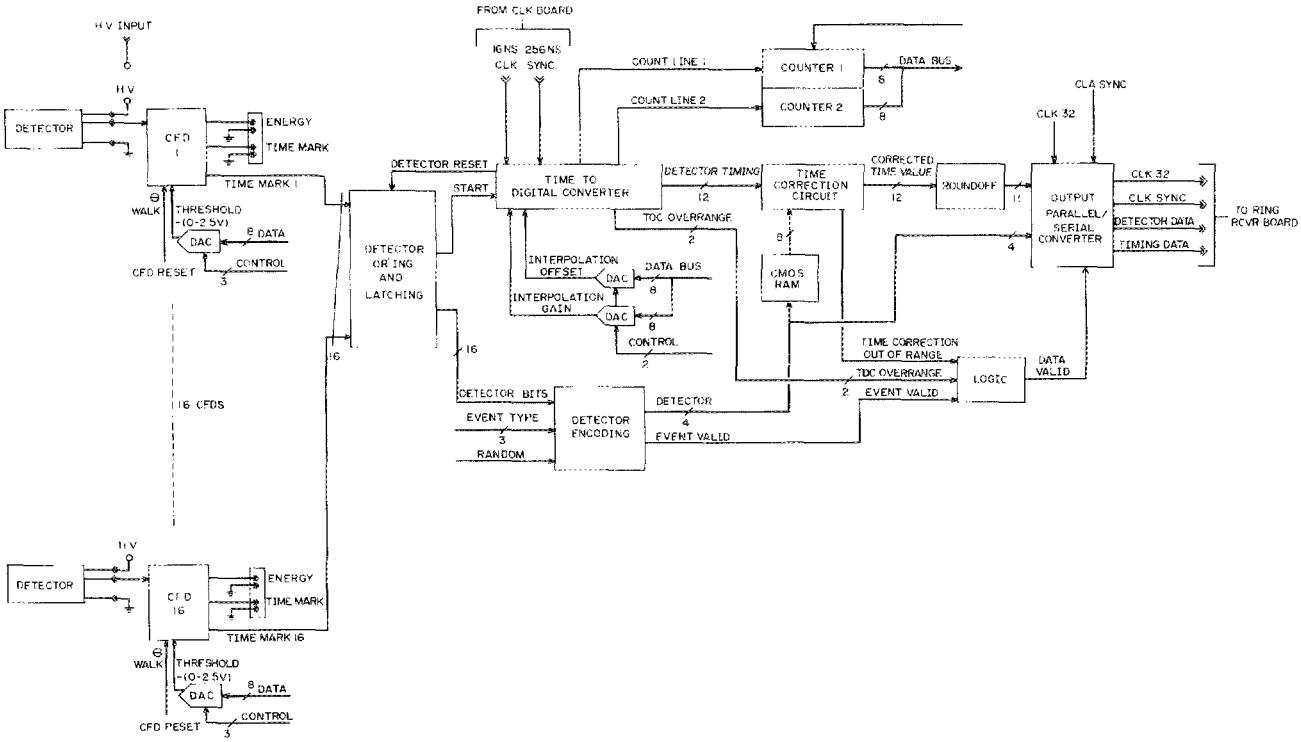


FIG. 3. Bucket electronics block diagram.

formation and the RTS is supplemented by a TOF formatter. Every 256 nanoseconds, the ring receiver accepts event data and transfers to the TOF coincidence processor which searches a coincidence pair within a time window (12 ns) and encodes them. Forty-eight line-of-responses (LORs) are adopted for obtaining a field-of-view (FOV) with 56 cm diam (see Fig. 4). The RTS calculates a detector position ($d$), view of angle ($\theta$) and time of flight from the center of gantry ($t$) by detector numbers ($N_1$ and $N_2$) and arriving time ($t_1$ and $t_2$) of a coincident event, and forms a three dimensional sinogram $E(d,\theta,t)$ into Versatile Module Europe (VME) solid-state memory (128 MB). The TOF formatter discriminates between $t = t_1 - t_2$ and $t_2 - t_1$ according to a geometric condition of $N_1$ and $N_2$. In our TOF-PET, the three dimensional sinograms can be formed simultaneously during emission scanning, while in other systems the event data are stored in a disk as a preliminary step and three dimensional sinograms are formed by the analysis of list data[22] after the scan.

### C. Data processing system

Three dimensional sinograms $E(d,\theta,t)$, sorted in solid-state memory of the data-acquisition system, are transferred into a data disk through a direct memory access (DMA) and rearranged into a form of $S_0(t,d,\theta)$ (described later). A minicomputer (DEC micro-VAX II) and array processors (Analogic AP500) perform an image reconstruction with the three dimensional sinogram and a display processor (Gould/De Anza FD5000) displays it on a video monitor. The programs of operation, maintenance, image reconstruction and other software are saved on a system disk.

## III. DATA ACQUISITION AND ITS STRUCTURE DEFINITION

### A. Acquisition mode

Two acquisition modes are available for requirements of low and high spatial resolution, the stationary and wobble modes, respectively.

#### *1. Stationary mode*

As seen in Fig. 4, we have 256 views of projection and 48 LORs for each view. By interpolating odd angle data into those of even angles, we can define a sinogram with 96 and 128 bins for $d$ and $\theta$, respectively.

#### *2. Wobble mode*

An improvement for spatial resolution is achieved by wobbling the gantry and sampling at four positions. The TOF sinogram with 192 and 256 bins for $d$ and $\theta$, respectively, is defined in this mode.

### B. Time structure definition

The present system provides 32 bins of TOF information as shown in Fig. 5. The bins 2-30 and 125 ps/bin (18.75 mm/bin) are used in the TOF sinogram $S_0(t,d,\theta)$, limiting the effective field of view to 543.75 mm. In a simultaneous measurement of emission and transmission data, events from a ring source are accumulated into bin 1 and 31 with a time window 1.75 ns. Random coincidence events in the final bin 32 are useful for a background subtraction.

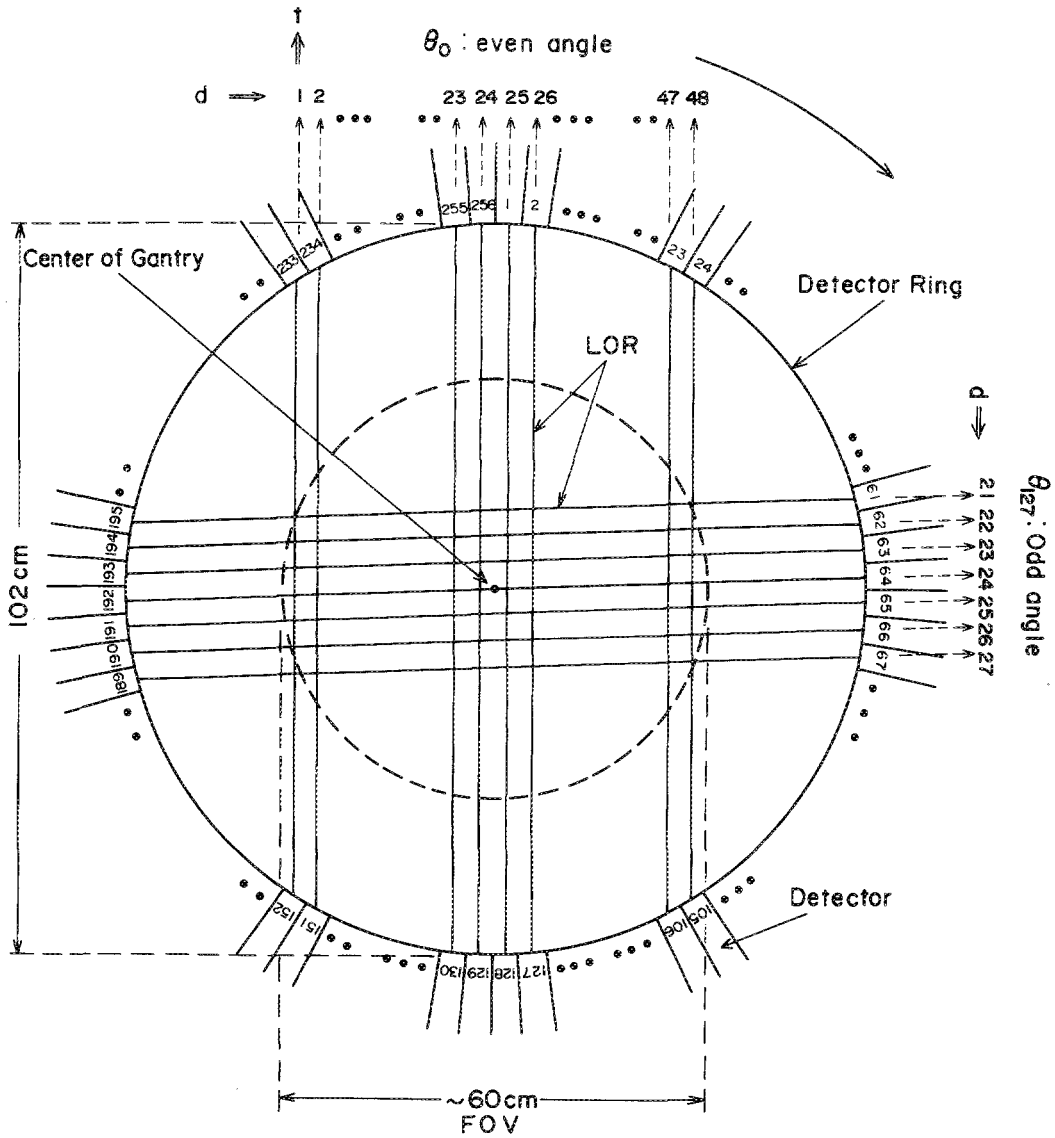


FIG. 4. Definition of line-of-responses (LOR). 48 LORs are defined along the detecting direction for a sinogram and 256 views are available in the present detector ring. There are two types of LORs, some passing through the center of gantry and some not passing through the center of the gantry.

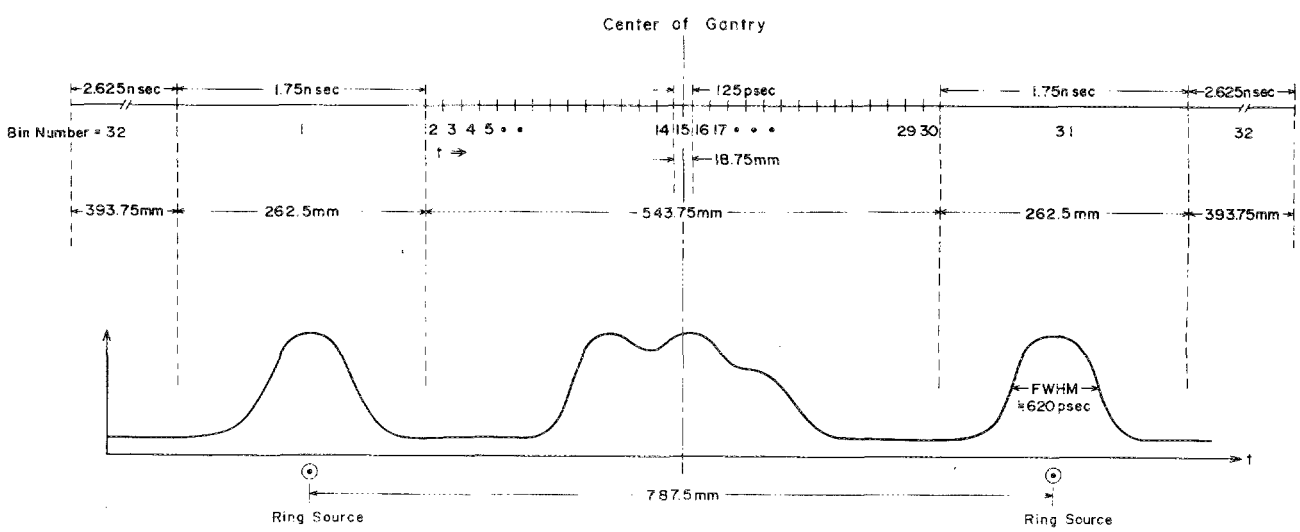


FIG. 5. Time data structure. The present system has 32 bins for storing time data. Bins No. 2-30 are used to the TOF sinogram, those of No. 1 and 31 for a ring source and No. 32 for random coincidence events.

## IV. TIME ALIGNMENT

The origin of all time axes in the TOF sinograms should be accurately adjusted on a line passing the center of gantry and perpendicular to the LORs, that is, the center locations of the LORs must be accurately adjusted. The misalignments between TOF positions will result in loss of image quality obtained by TOF information and also result in a distortion of the image. On the TOF-PET systems so far reported, the time alignment has been achieved with a ring source. In these PETs, the peaks of TOF distribution corresponding to the positions of ring source are measured and the TOF time axes are corrected when three dimensional sinograms are formed.[22] This method requires very large memories for the three dimensional sinograms, since more than ten bins on the time axis are required just for the measurement of the ring source. On the other hand, as seen in Fig. 5, two wide bins on the time axis are enough to obtain the transmission data with the ring source, but these two bins are too wide to be used for time alignment. All detectors in a ring are symmetric with each other and their axes may be aligned using a standard detector separated from them. This method is simple, but much software and hardware relating to the standard detector is required. We found a unique method requiring no additional detector hardware.

When a semiring source with a diameter of one half the detector ring is placed as shown in Fig. 6(a), the source is located at the center of the LORs. The time spectrum for each LOR is fitted with a Gaussian-type function and a deviation from center (i.e., offset time) is estimated with accuracy. By feeding the offset values in units of 62.5 ps into the time digitizer, detectors 85 ~ 171 can be aligned to the detector 1. The alignments for remaining detectors 2 ~ 84 and 172 ~ 256 are carried out with rotating the semiring source as shown in Fig. 6(b) and (c), respectively. Reference detector 1, 85 and 171 can be more accurately aligned with the use of plane source due to its symmetry [see Fig. 6(d)]. This method can perform the time alignment within an accuracy of $\pm$ 31.25 ps.

## V. CORRECTION DATA

A measured sinogram $S_0(t,d,\theta)$ should be corrected for detector efficiencies and attenuation within the patient

$$S(t,d,\theta) = S_0(t,d,\theta) \times N(d,\theta) \times A(d,\theta), \tag{2}$$

where $N(d,\theta)$ and $A(d,\theta)$ are called normalization data and attenuation data, respectively.

### A. Normalization data

The same method as the PT931 conventional PET systems used to obtain the normalization data, where a plane source is measured at six angles in stationary mode and detection efficiency data is constructed with its sinograms summed up by time bins (that is non-TOF mode). The normalization data for the wobble mode is calculated from those obtained by the stationary mode. TOF resolutions (FWHM) with respect to every time axis are obtained from the TOF sinograms of normalization data, since the averaged value $\Delta T$ is required in a calculation of TOF filter function $g_{\mathrm{TOF}}(d)$:

$$g_{\mathrm{TOF}}(d) = \sqrt{\frac{\pi}{ln\,2}}\,\Delta t g_o(d) e^{-\left(\frac{d}{\Delta t}\right)^2 ln\,2} \tag{3}$$

and

$$\Delta t = \Delta T x \frac{C}{2},$$

where $g_o(d)$ is a filter function for a conventional PET.[23,24]

### B. Attenuation data

The absorption of positron $\gamma$-rays with a patient is measured by the use of ring source uniformly filled with a $^{68}$Ge radioisotope solution. The attenuation data $A(d,\theta)$ is given from dividing blank data $B(d,\theta)$, measuring only the ring source, by a transmission data $T(d,\theta)$, measuring the ring source with a patient: $A(d,\theta) = B(d,\theta)/T(d,\theta)$. The blank data should be obtained independently of the emission data $S_0(t,d,\theta)$, however, the transmission data can be acquired at the same time due to the TOF technique. This simultaneous

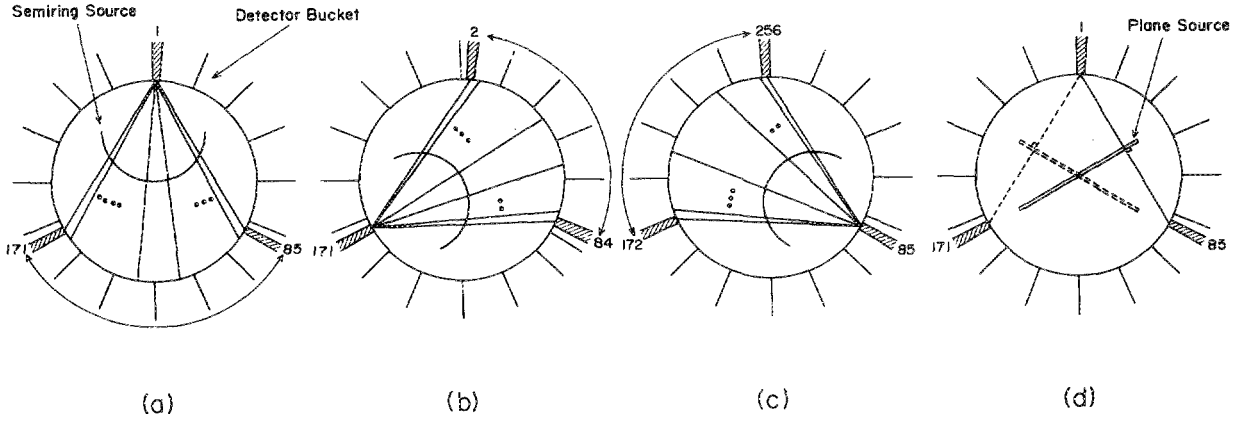


FIG. 6. Time alignment routine. Using a semiring source, all detectors can align their time axes with that of the detector 1 by the process of (a) → (b) → (c). A more accurate alignment of reference detectors of No. 171 in (b) and No. 85 in (c) is achieved with a plane source in (d).

measurement is difficult to obtain in the case of conventional PET.[25] A large diameter 787.5-mm ring source is adopted in consideration of an interference effect between the ring source and body (see Fig. 5).

## VI. IMAGE RECONSTRUCTION

The emission data $S_0(t,d,\theta)$ is smoothed with respect to the time axis in order to reduce statistical noise. This smoothing process consists of a weighted average with adjacent time data

$$S_0(I,J,K) \leftarrow [S_0(I-1,J,K) + 2\times S_0(I,J,K) + S_0(I+1,J,K)]/4.0. \quad (4)$$

The corrections for detector efficiency and absorption then are made with Eq. (2). Actual detector positions far from the center of gantry are not proportional to their bin number. The present reconstruction software corrects this by,

$$S(I,J,K) \leftarrow S(I,J,K) + [S(I,J+1,K) - S(I,J,K)] \times [J - d(J)]/[d(J+1) - d(J)], \quad (5)$$

where $d(J)$ is an actual detector position which can be obtained by calculation or measurement. After such corrections, a convolution between the TOF sinogram $S(t,d,\theta)$ and a filter function $g_{\mathrm{TOF}}(d)$ is carried out and an image is reconstructed by the method previously reported.[16] It is noticed here that, in the case of wobble mode, the origin of time axis moves within a wobble circle. We may however neglect this effect on the image reconstruction, since the wobble diameter (1 cm) is very small compared with a reduced length of TOF resolution (600 ps→9 cm). The effective time resolution depends on the mean square combination of all errors and is dominated by the detector timing resolution. A flow chart for processing TOF image reconstruction is presented in Fig. 7.

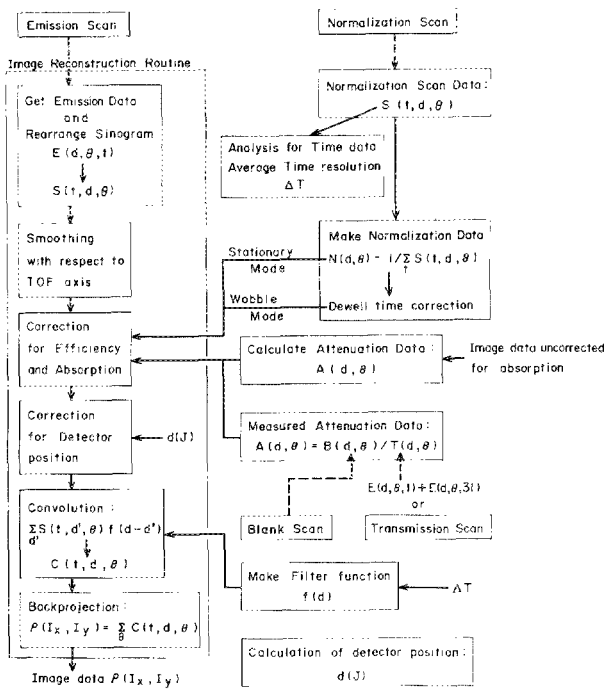


FIG. 7. Flow chart of the image reconstruction programs.

## VII. PERFORMANCE CHARACTERISTICS

### A. Scan mode

The TOF-PET provides four scan modes for clinical studies.

#### *1. Static emission scan*

Emission data can be acquired as a function of bed position. Different acquisition times are available for each frames.

#### *2. Dynamic emission scan*

Fixing bed position, a dynamic study can be carried out with frames of time intervals.

#### *3. Gated emission scan*

Cardiac study is available where a maximum of 160 and 40 gated acquisitions are available for stationary and wobble mode, respectively.

#### *4. Direct imaging scan*

Using the TOF-PET, the position of positron radioisotopes can be localized within an accuracy of its time resolution. In other words, the TOF sinograms $s(t,d,\theta)$ directly represent a positron image viewed at an angle $\theta$. This feature enables us to obtain a significant image even with statistically insufficient data measured in a very short time interval. This mode is useful to observe very fast density distribution changes in a body (for an example, motion of positron isotopes). The present TOF-PET provides us "movie" images of 15 s with 0.1 s/frame.

### B. Spatial resolution

The $^{68}$Ge needle source of stainless-steel tube with an inside diameter of 1.4 mm and outside diameter of 1.8 mm was used to measure the spatial resolution. Figure 8 shows

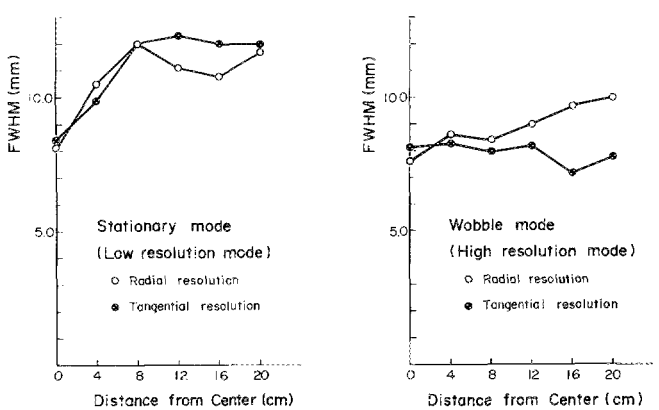


FIG. 8. Spatial resolution of TOF-PET as a function of distance from the center of gantry.

the spatial resolutions as a function of distance from the center of gantry. By the use of wobble mode, we did achieve a high resolution TOF-PET with a spatial resolution of 8-mm FWHM. The axial resolution was also measured and was 9.65-mm FWHM.

### C. Time resolution

An average system resolution of 623 ps FWHM ($1/2\ \Delta T \times C = 9.2$ cm) has been obtained within a deviation of 55 ps. Though this value is larger than the 470 ps FWHM ($1/2\ \Delta T \times C = 7.0$ cm) reported for the Super PETT and TTV01 TOF PETs, the slightly higher time resolution is not a significant disadvantage. As mentioned, the TOF-PET reported here features better (smaller) detector sampling and corresponding higher spatial resolution.

### D. Sensitivity and uniformity

A uniformly distributed source of 21 mCi $^{18}$F contained in for a $20\times20$-cm-deep cylindrical phantom has been used to measuring sensitivity and uniformity. We obtained a sensitivity of 4054 cps/$\mu$Ci/ml with a deviation of $\pm$ 5.8%.

### E. Image quality

A cylindrical phantom has been measured in order to examine the improvement in image quality with the use of TOF information. The cylindrical phantom was divided into three layers of which diameters were 26 mm, 150 mm and 200 mm for center, inside and outside, respectively. The central and outside regions were filled with $^{18}$F activated water of 0.92 $\mu$Ci/cc and 8.5 $\mu$Ci/cc, respectively. The inside region was filled with normal water. The measurement was done for two minutes in stationary mode. Figure 9 shows the reconstructed images. The TOF image was reconstructed on the basis of Eq. (6) in Ref. 16, which is a straightforward method compared with the one[22] used in other TOF-PETs. The NON-TOF image was obtained by a usual method [Eq. (4) in Ref. 16] by integrating the TOF sinogram used in the TOF image over the time axis. We can see a clear difference in image quality between them. The outside ring is well reproduced in the TOF image, but, in the case of NON-TOF image, its image is considerably affected with the artifacts

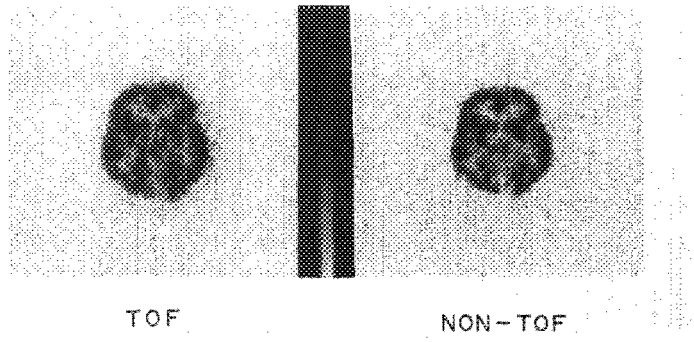


FIG. 10. Effect of using TOF informations in an example of human brain.

due to the central region. This result is of course an effect of the use of TOF information. The outside region is separated by 6 cm from the central region and the present resolution of TOF corresponds to 9 cm. Therefore, in this case, the outside region and central region hardly interact with each other in the TOF reconstruction.

The $^{18}$FDG images of a middle part of human head are shown in Fig. 10 where the $^{18}$FDG solution of 8.3 mCi was injected, and, after 90 minutes, data was acquired in wobble mode for thirty minutes. Both TOF and NON-TOF images were generated as in Fig. 9. It is seen in comparison between them that the TOF-PET reproduces positron images with high confidence: The TOF image is superior in the view of reproducing the contrast in density,[8] the parts lacked in the NON-TOF image (e.g. the occipital region) can be seen and a structure of interior is well reproduced in the TOF image.

Figure 11 presents the TOF images of upper part of head measured by stationary and wobble mode, respectively. Though the improvement in resolution is still required for the image of stationary mode, it will be useful for some applications.

For the absorption of $\gamma$-rays, the $BaF_2$ scintillator is less dense than the BGO scintillator. For this reason, the spatial resolution of conventional BGO-PET is superior to that of TOF-PET. If a denser (denser than $BaF_2$) scintillator producing fast timing pulses is developed or discovered, the image quality of TOF-PET will be improved by the effect of TOF information coupled with the high spatial resolution of

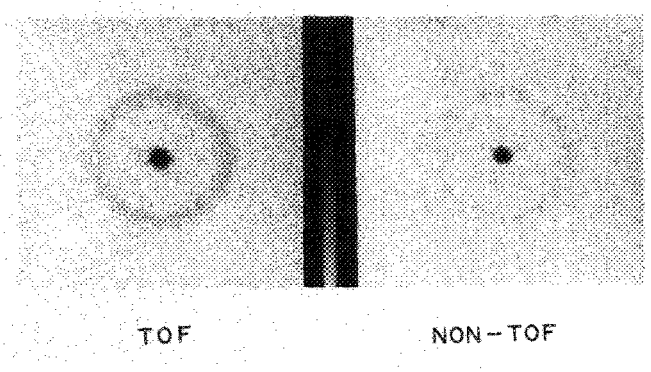


FIG. 9. Examination of image quality with a cylindrical phantom divided into three layers. non-TOF and TOF show the images reconstructed without and with the use of TOF informations, respectively.

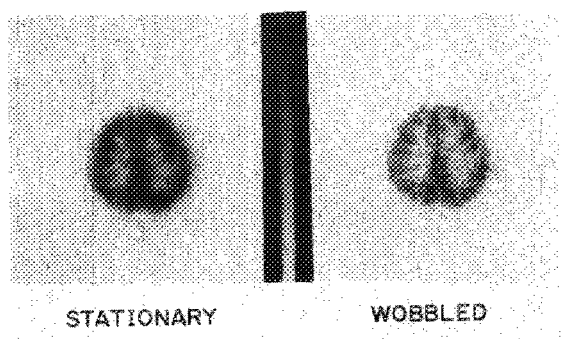


FIG. 11. Comparison between images obtained with stationary and wobble modes; $^{18}$FDG images of upper part of human head.

a denser scintillator. Since the spatial resolution of PET is limited by the range of positrons in a material, PET spatial resolution will however not be better than non-PET tomographs such as X-CT and MRI.

The high performance TOF-PET described here is now being used for clinical studies on tumors, cardiac disease, brain infarction, dementia, etc. along with the conventional PETs (PT931 and ECATII) and other CT machines (MRI and X-CT) at the Research Institute for Tuberculosis and Cancer.

## ACKNOWLEDGMENTS

The authors would like to thank our collaborators who have contributed to this work. T. Jansto worked on the development of software for data acquisition and M. Tominaga, M. Takahashi and A. Fujimoto assisted us in developing the software for data processing. C. Williams made efforts in coupling the photomultiplier to $BaF_2$ crystal with RTV. Dr. J. Hatazawa accepted to be a first volunteer for our TOF-PET. Dr. R. Iwata and his co-workers readily supplied us the radioisotope products of $^{18}F$. S. Watanuki aided us well in the measurements and examination of TOF-PET. Our thanks are also presented to staffs of Cyclotron and Radioisotope Center and CTI who have supported this work.

[1]M. M. Ter-Pogossian, M. E. Phelps, and E. J. Hoffman, Radiology **114**, 89 (1975).
[2]M. E. Phelps, E. J. Hoffman, N. A. Mullani, and M. M. Ter-Pogossian, J. Nucl. Med. **16**, 210 (1975).
[3]R. A. Brooks and G. Dichiro, Phys. Med. Biol. **21**, 689 (1976).
[4]M. Reivich and A. Alarri, *Positron Emission Tomography* (Alan R. Liss, Inc., New York, 1985).
[5]F. Soussaline, D. Comar, R. Allemand, R. Campagnolo, M. Laval and J. Vacher, *The Metabolism of the Human Brain Studied with Positron Emission Tomography*, edited by T. Greitz *et al.* (Raven, New York, 1985), pp. 1–11
[6]N. A. Mullani, J. Markham, and M. M. Ter-Poggossian, J. Nucl. Med. **21**, 1095 (1980).
[7]M. M. Ter-Pogossian, N. A. Mullani, D. C. Ficke, S. Murkham, and D. L. Snyder, J. Comput. Assist. Tomogr. **5**, 227 (1981).
[8]M. M. Ter-Pogossian, D. C. Ficke, M. Yamamoto, and J. T. Hood, IEEE Comput. Soc. Pub. **37**, 488 (1983).
[9]R. Allemand, C. Gresset, and J. Vacher, Nucl. Med. **21**, 153 (1980).
[10]R. Compagnolo, M. Laval, M. Moszynski, and F. Soussaline, Laboratoires Mesure, Controle et Traitement Electronique (MCTE)/82-353, 1982
[11]M. Laval, M. Moszyski, R. Allemand, E. Cormoreche, P. Guinet, R. Odru, and J. Vacher, Nucl. Instrum. Meth. **206**, 169 (1983).
[12]T. K. Lewellen, M. D. Pencke, A. N. Bice, and R. L. Harrison, IEEE Trans. Nucl. Sci. **35**, 726 (1988).
[13]T. K. Lewellen, A. N. Bicc, R. L. Harrison, M. D. Pencke, and J. M. Link, IEEE Trans. Nucl. Sci. **35**, 665 (1988).
[14]Time-of-flight positron emission tomograph, whole body tomograph-TTV-03, Laboratoires Mesure, Controle et Traitement Electronique (MCTE)/85-359, 1985.
[15]K. Ishii, S. Watanuki, H.. Orihara, M. Itoh, and T. Matsuzawa, Nucl. Instrum. Meth. A **253**, 128 (1986).
[16]K. Ishii, H. Orihara, and T. Matsuzawa, Rev. Sci. Instrum. **58**, 1699 (1987).
[17]D. Binkley and M. E. Casey, IEEE Trans. Nucl. Sci. **35**, 226 (1988).
[18]H. M. Dent, W. F. Jones, and M. E. Casey, IEEE Trans. Nucl. Sci. **33**, 556 (1986).
[19]W. F. Jones, M. E. Casey, L. G. Byars, and S. G. Burgiss, IEEE Trans. Nucl. Sci. **33**, 601 (1986).
[20]Technical Description of MODEL 931 ECAT SCANNER, Computer Technology & Imaging, Inc., Knoxville, TN, May 1986.
[21]N. A. Mullani, W. H. Wong, R. K. Hartz, K. Yerian, E. A. Philippe, and K. L. Goudl, Proc. Workshop TOF Tomography, IEEE Com. Soc., St. Louis, 31 (1982).
[22]M. Yamamoto, G. R. Hoffman, D. C. Ficke, and M. M. Ter-Pogossian, IEEE Com Soc Pub, Workshop on Time-of-Flight Tomography, 125 (1983).
[23]D. A. Chesler and S. J. Riederer, Phys. Med. Biol. **20**, 632 (1975).
[24]E. Tanaka and T. A. Iinuma, Phys. Med. Biol. **5**, 789 (1975).
[25]M. E. Daube-Witherspoon, R. E. Carson, and M. V. Green, IEEE Trans. Nucl. Sci. **31**, 757 (1988).